# The antioxidative potential of procyanidin B1: DFT (density functional theory) and docking approaches

**Article** *in* Journal of Molecular Modeling · March 2023

DOI: 10.1007/s00894-022-05354-x

CITATIONS
0

READS
24

**4 authors:**

Phan Thi Thuy
Vinh University
**19** PUBLICATIONS **76** CITATIONS
SEE PROFILE

Quan Minh Pham
Vietnam Academy of Science and Technology
**116** PUBLICATIONS **804** CITATIONS
SEE PROFILE

Dau Duc
Vinh University
**27** PUBLICATIONS **86** CITATIONS
SEE PROFILE

Son Ninh The
Vietnam Academy of Science and Technology
**95** PUBLICATIONS **564** CITATIONS
SEE PROFILE

Journal of Molecular Modeling (2022) 28:356
https://doi.org/10.1007/s00894-022-05354-x

ORIGINAL PAPER

# The antioxidative potential of procyanidin B1: DFT (density functional theory) and docking approaches

**Phan Thi Thuy[1] · Pham Minh Quan[2] · Dau Xuan Duc[1] · Ninh The Son[3]**

Received: 3 July 2022 / Accepted: 6 October 2022


## Abstract

Procyanidin B1 is one of the natural dimeric flavonoids. It has established a great role in antioxidative activity. In the current study, we wish to provide crucial information on its antioxidative action by the DFT computational and docking approaches. From point of thermodynamic view, at the M062X/6-311G(d,p) level, the HAT (hydrogen atom transfer) and SPL-ET (sequential proton loss-electron transfer) are principal antioxidative routes of this compound in gas and methanol, respectively. OH groups of two phenyl rings of this molecule are likely to be the best antiradical sites. In the kinetics of the interactions with $HOO^{\bullet}$ radicals, OH groups of phenyl rings have also generated the best $\Delta G^{\#}$ (Gibbs free energy of activation) and rate constant *K*. The antioxidative action of procyanidin B1 is further confirmed by its chelation to metal ions, in which complex formation with $Cu^{2+}$ having lower binding energy is more stable than complex formation with $Zn^{2+}$. Docking study revealed that the antioxidative activity of procyanidin B1 involved human tyrosinase enzyme inhibition through interaction with essential residues, focusing on the OH groups of two phenyl rings.

**Keywords** Procyanidin B1 · Antioxidant · Density functional theory · Docking

## Introduction

Procyanidins, also referred to as proanthocyanidins, are one of the most beneficial chemical classes of flavonoids [1]. They have been categorized as oligomeric compounds, and were structurally formed from catechin and epicatechin units [2]. Many herbaceous plants, such as apple, cocoa bean, green tea, and grape, are the rich resources [3]. Procyanidin derivatives established a great role in food chemistry because their antioxidative activity against free radicals was 30–50 times higher than vitamins C and E [4, 5].

Procyanidin B1 (PB1) is a dimeric molecule, comprising of (+)-catechin and (−)-epicatechin units connected via 4β → 8″ bond (Fig. 1). This metabolite can be detected in many plants, such as *Cinnamomum verum*, *Prunus persica*, *Uncaria guianensis*, and *Vitis vinifera* [6, 7]. Various reports identified that PB1 is considered as a promising antioxidant agent. In the antioxidant assay against DPPH radical, PB1 has induced the $EC_{50}$ value of $3.2 \times 10^{-6}$ M much lower than that of the positive controls resveratrol, ascorbic acid, and trolox ($11.8–31.4 \times 10^{-6}$ M) [8]. In another antioxidant assay measured by TEAC (trolox equivalent antioxidant capacity), FRAP (ferric-reducing antioxidant power), and HOCl (hypochlorous acid) methods, PB1 reached the respective $IC_{50}$ values of 6.55, 11.85, and 15.12 mM, as compared with those of ascorbic acid ($IC_{50}$ 1.42, 2.26, and 427.62 mM) [9].

Although there have been increasing numbers of experimental studies on the antioxidant of PB1, the computational approaches to shed light on the most active sites in this molecule are very limited. Our current study uses DFT calculation to estimate the OH bond breakage energies and kinetics of compound PB1 [10–14]. Furthermore, tyrosinase enzyme is a well-known target for antioxidative drug development, in which it participated in three stages of melagonesis at least [15]. It promoted L-DOPA by hydroxylation. Also, it catalyzed the oxidation of 5,6-dihydroxyindole to form indole-5,6-quinone. Based on these findings, molecules that

✉ Ninh The Son
yamantson@gmail.com

[1] Faculty of Chemistry, College of Education, Vinh University, 182 Le Duan, Vinh, Nghean, Vietnam

[2] Institute of Natural Products Chemistry, Vietnam Academy of Science and Technology (VAST), 18 Hoang Quoc Viet, Caugiay, Hanoi, Vietnam

[3] Institute of Chemistry, Vietnam Academy of Science and Technology (VAST), 18 Hoang Quoc Viet, Caugiay, Hanoi, Vietnam

Published online: 12 October 2022

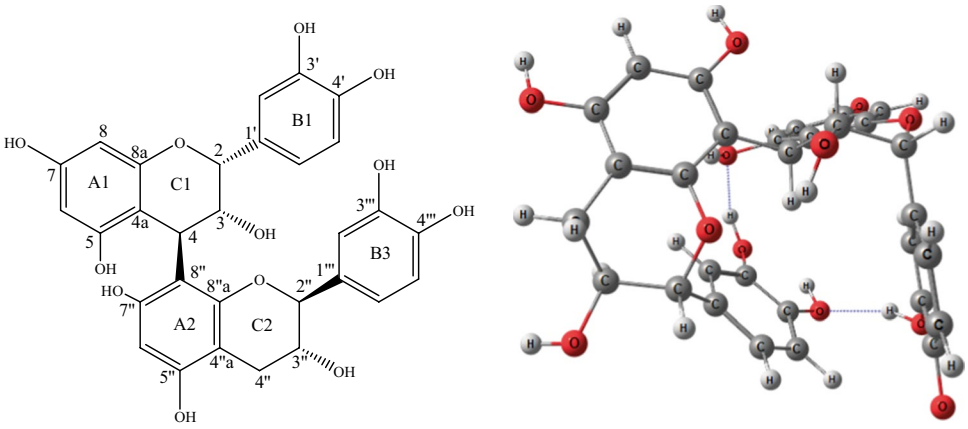


**Fig. 1** General structure of procyanidin B1 (PB1) with atom numbering and its optimized form at the theoretical M06-2X/6-311G(d,p) level

inhibited tyrosinase would block melanin biosynthesis and were used for the treatment of skin blemishes [16]. Thus, we aim to investigate the inhibitory potential of PB1 against tyrosinase enzyme by docking study.

## Theoretical methodology

### DFT computational studies

The DFT computational procedures were administered using the functional M062X [17]. Geometrical processes regarding molecule PB1-OH and its derivatives PB1-O$^{\bullet}$, PB1-OH$^{\bullet+}$, and PB1-O$^{-}$ have been fully optimized at the M062X/6-311G(d,p) level utilizing the Gaussian 09 W package [18]. To ensure accuracy, harmonic frequency calculations were carried out to validate ZPE corrections and stationary points, at the same M062X/6-311G(d,p) level. The computational polarizable continuum solvation model was extensively applied to theoretically estimate solvent effects.

The free radical scavenging by antioxidant molecule PB1-OH can be performed through three different processes, consisting of HAT, SET-PT, and SPL-ET [19–23].

a) The HAT process, also known as hydrogen atom transfer, is due to the abstraction of a proton from PB1-OH, and quickly transfers to the radical A$^{\bullet}$ (Eq. (1)). This reaction has been classified as a homolytic action, and has been considered by the BDE (bond dissociation energy) (Eq. (2)).

$$\mathrm{PB1-OH + A^{\bullet} \rightarrow PB1-O^{\bullet} + AH} \quad (1)$$

$$\mathrm{BDE = E(PB1-O^{\bullet}) + E(H^{\bullet}) - E(PB1-OH)} \quad (2)$$

b) The SET-PT process contains the single-electron transfer (SET) and the proton transfer (PT). As shown in Eq. (3), the electron loss from PB1-OH to PB1-OH$^{\bullet+}$ represents the SET, and can be recognized by the AIP (atomic ionization potential) (Eq. (4)). After the SET, PB1-OH$^{\bullet+}$ has been further deprotonated, and this action can be characterized by the PDE (proton dissociation enthalpy) (Eq. (5)).

$$\mathrm{PB1-OH + A^{\bullet} \rightarrow PB1-OH^{\bullet+} + A^{-} \rightarrow PB1-O^{\bullet} + AH} \quad (3)$$

$$\mathrm{AIP = E(PB1-OH^{+\bullet}) + E(e^{-}) - E(PB1-OH)} \quad (4)$$

$$\mathrm{PDE = E(PB1-O^{\bullet}) + E(H^{+}) - E(PB1-OH^{\bullet+})} \quad (5)$$

c) The SPL-ET process is caused by the sequential proton loss (SPL), and then the electron transfer (ET). In the first action (Eq. (6)), PB1-OH is converted into PB1-O$^{-}$ by deprotonation, whereas the second process involves electron delivery from PB1-O$^{-}$ to the radical A$^{\bullet}$. It turns out that the PA (proton affinity) and ETE (electron transfer enthalpy) are applied to consider energy for the first and second processes, respectively (Eqs. (7) and (8)).

$$\mathrm{PB1-OH \rightarrow PB1-O^{-} + H^{+}; PB1-O^{-} + A^{\bullet} \rightarrow PB1-O^{\bullet} + A^{-}; A^{-} + H^{+} \rightarrow AH} \quad (6)$$

$$\mathrm{PA = E(PB1-O^{-}) + E(H^{+}) - E(PB1-OH)} \quad (7)$$

$$\mathrm{ETE = E(PB1-O^{\bullet}) + E(e^{-}) - E(PB1-O^{-})} \quad (8)$$

$E(N)$ represents the total enthalpy of the species $N$ in the DFT calculation, and it can be represented as Eq. (9) [19].

$$E(N) = Q + \mathrm{ZPE} + \Delta E_{\mathrm{trans}} + \Delta E_{\mathrm{rot}} + \Delta E_{\mathrm{vib}} + \mathrm{RT} \quad (9)$$

where $Q$ and ZPE represent the respective electronic and zero-point energies. The $\Delta E_{\mathrm{trans}}$, $\Delta E_{\mathrm{rot}}$, and $\Delta E_{\mathrm{vib}}$ display

the translational, rotational, and vibrational contributions to enthalpy, respectively. The $E(e^-)$ and $E(H^+)$ were extracted from previous reports [19].

The Fukui function denotes the electron density after accepting or denoting an electron, by which it may estimate where the most nucleophilic ($f_x^-$), electrophilic ($f_x^+$), or radical ($f_x^o$) sites on a substance are Eqs. (10)–(12) [23].

$$f_x^+ = R_X(M+1) - R_X(M) \tag{10}$$

$$f_x^- = R_X(M) - R_X(M-1) \tag{11}$$

$$f_x^o = [R_X(M+1) - R_X(M-1)]/2 \tag{12}$$

where $R$ stands for the total charge of atom. The electronic populations of an atom in neutral, anionic, and cationic forms are $P_X(M)$, $P_X(M+1)$, and $P_X(M-1)$, respectively.

The conventional TST (transition state theory) was employed to view the kinetic aspect of a radical reaction [20, 21]. At $T=300$ K and the M062X/6-311G(d,p) level, the rate constant $K$ has induced a relation to the $\Delta G^{\#}$ (Gibbs free energy of activation) as shown in the next equation (Eq. (13)).

$$k(T) = \kappa \frac{T.k_B}{h} e^{\frac{-\Delta G^{\#}}{RT}} \tag{13}$$

where $\kappa$, $h$, and $k_B$ denote the Wigner coefficient and the Plank and Boltzmann constants, respectively.

### Docking studies

The molecular docking study utilized AutoDock 4.2.6 with Lamarckian genetic algorithm (LGA) for searching the optimized dock pose together with a scoring function to calculate the binding affinity. The three-dimensional structure of PB1 was prepared using MarvinSketch version 19.27.0 and PyMOL version 1.3r1 [24]. Subsequently, geometry minimization was carried out using DG-AMMOS with default setting [25]. The energy minimization of the ligand was performed using Gabedit version 2.5.0 [26]. The X-ray crystal structure of human tyrosinase-related protein was achieved from the Protein Data Bank archive (PDB) with entry ID: 5M8M [27]. A natural occurring tyrosinase inhibitor, kojic acid (KA), is selected as a reference ligand [28].

It assumed that the protein is rigid and the conformational space of the ligands to analyze the inductive effect of the compounds is considered. AutoDockTools were utilized to prepare protein for docking simulations. The heteroatoms including water molecules were deleted and polar hydrogen atoms and Kollman charges were added to the receptor molecule. All other bonds were allowed to be rotatable. In the docking analysis, the binding site was enclosed in a box with the number of grid points in $x \times y \times z$ directions ($56 \times 56 \times 56$) and a grid spacing of 0.375 Å. The center of grid box was assigned as $x = -33.215$, $y = -0.292$, and $z = -26.008$ to involve the active site of receptor which was constituted by residues His192, Val196, Tyr362, Arg374, His377, His381, Thr391, and Ser394 [29–31]. Initially, AutoGrid was run to generate the grid map of various atoms of the ligands and receptor. After that, AutoDock was run by using autodock parameters as follows: GA population size, 300; maximal number of energy evaluations, 25,000,000; and the number of generations, 27,000. A maximal number of 50 conformers were considered for each molecule, and the root-mean-square (RMS) cluster tolerance was set to 2.0 Å in each run.

## Results and discussion

### Geometrical analysis

The effects of radical quenching reactions are highly influenced by the chemical structural features such as bond distance, and geochemistry, particularly the fluctuation of OH groups [19]. In this section, we briefly describe geometrical analysis for molecule PB1. Figure 1 and Table S1 provide information on the optimized structure of compound PB1 in gas, water, methanol, and benzene at the M062X/6-311G(d,p) level. The $\pi$-electrons are found to be delocalized in aromatic rings A1, A2, B1, and B2, but they are completely absent in rings C1 and C2. The co-planarity between chromene and phenyl rings and between two chromene rings is lost; thereby the dihedral angle $\theta$ (C3-C4-C8″-C8″a) reached averagely − 93.25°. It is also viewed that 3′-OH and 3‴-OH have hydrogen bonds with OH-4‴ and OH-5, respectively. In contrast to the 3′-OH…OH-4‴ bond, the 3‴-OH…OH-5 bond seems to be more durable in nonpolar or weak solvents (Table S1). Except for the cases of 4′(O–H), 7″(O–H), and 4‴(O–H), the O–H bond lengths in the remaining cases have been dropped by 0.001–0.004 Å.

In order to establish the relative position between (+)-catechin and (−)-epicatechin, a curve of the dependence of energy on the dihedral angle $\theta$ was designed (Fig. 2), in which the energy of each conformer was obtained when $\theta$ changed in a step of 10° (Table S2). At the M062X/6-31G(d,p) theoretical level, the absolute minimal conformer is located at − 90°, whereas the local conformers have been established at − 70, − 10, 60, 150, and 170° with the relative energy $\Delta E$ values of 1.013, 3.080, 1.625, and 8.404 kcal/mol, respectively. In the meantime, the interchangeable barriers are found to peak at − 150, − 80, − 50, 50, 130, and 160° with the $\Delta E$ values of 11.374, 1.328, 5.749, 9.735, 15.725,

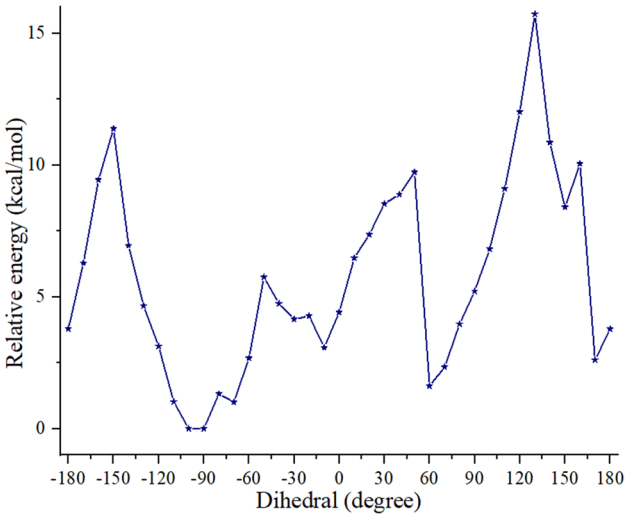


**Fig. 2** Potential energy curve versus the dihedral angle $\theta$ (C3-C4-C8″-C8″a) in gas at the theoretical M06-2X/6-311G(d,p) level

and 10.054 kcal/mol, respectively. Taken together, it suggests that the geometrical and electronic properties and OH behavior may decide the differences in anti-oxidative results.

## Frontier molecular orbital theory (FMO) and molecular electrostatic potential (MEP)

The FMO analysis is a prompt and crucial approach that considers the antioxidant of organic molecules [32]. Band gap energy $\varepsilon_{gap}$ demonstrates the donated capacity of electrons, and the HOMO shape elucidates the preferential sites for radical attack [32]. As shown in Fig. 3, the $\varepsilon_{gap}$ values rank in an order of gas < benzene < methanol < water. It can be concluded that medium solvent methanol and polar solvent water have greatly affected the processes to form PB1-$OH^{\bullet+}$ and PB1-$O^{-}$, while weak polar or nonpolar mediums support the homolytic processes [33]. The HOMO and LUMO illustrations of neutral and radical forms are not different when converted gas into benzene, methanol, and water (Figs. 3 and

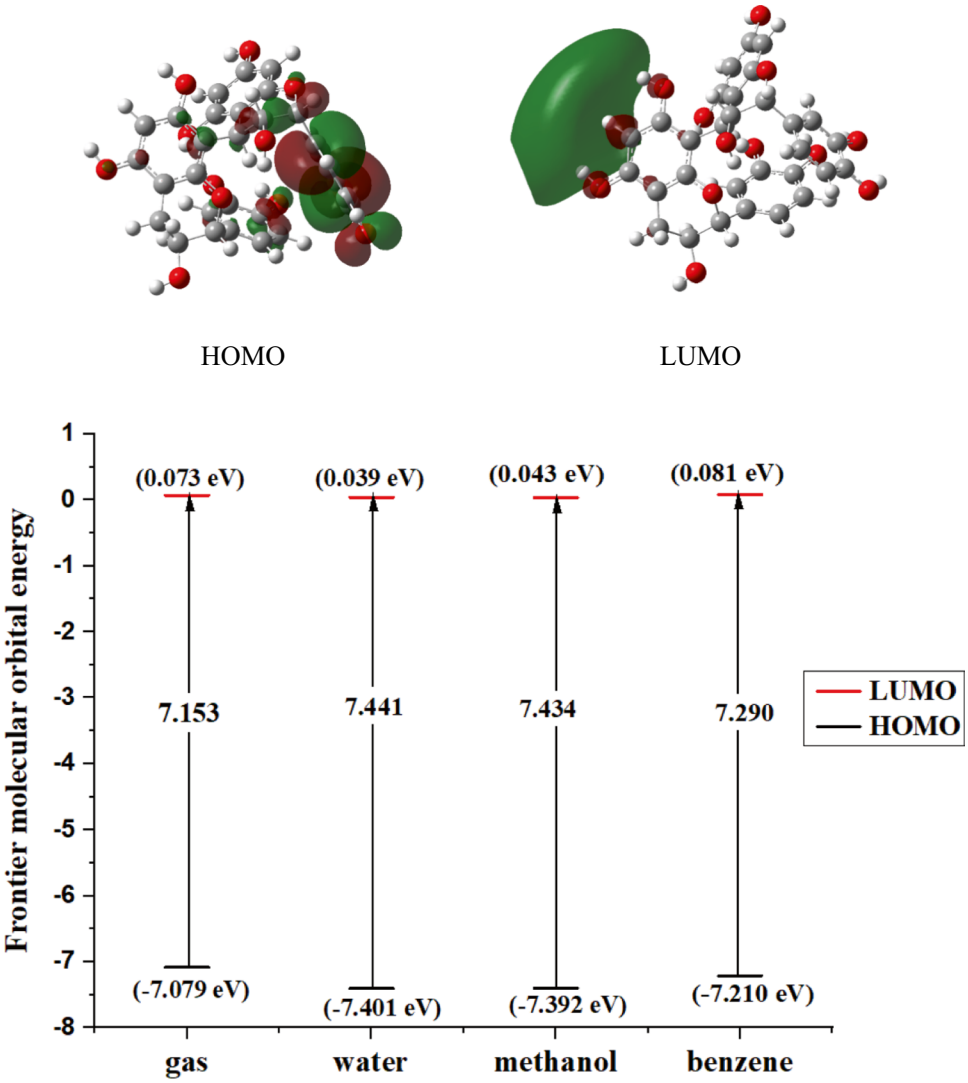


**Fig. 3** HOMO and LUMO images of neutral form in all studied mediums and band gap energy $\varepsilon_{gap} = \varepsilon_{HOMO} - \varepsilon_{LUMO}$ at the theoretical M06-2X/6-311G(d,p) level

S1). The neutral HOMO picture is characterized by electron delocalization in phenyl ring B1, and a little in 3‴-OH and 4‴-OH groups (Fig. 3). Regarding radicals, almost cases have been associated with the high electron concentration in two phenyl rings B1 and B2 (Fig. S1). Hence, two aromatic phenyl rings seem to facilitate antioxidative reactions better than chromene nuclei.

The MEP illustration was used as a map to visualize charged regions (the electron deficiency and excess) of each atom in a molecule [33]. The charged potentials have closely related to the color order: blue > green > yellow > orange > red, in which blue stands for the most positive charge, whereas orange and red conjugate with the most negative charge [33]. Green deduces from zero charge. From Fig. S2, oxygenated atoms are in conjunction with yellow; aromatic carbons and hydrogens are accompanied by green or blue. By means of this, OH groups played as appropriate sites for free radical attack [32].

## Spin density and Fukui analysis

The spin density is also one of the crucial criteria to evaluate the stability of radicals [20, 21]. In a conjugated molecule, the unpaired electron is more flexible, and the energy will be decreased [34]. Figure 4 exhibits the gaseous spin density of the O and C atoms after the H-extraction at the M062X/6-311G(d,p) level. In general, the spin is concentrated in aromatic rings higher than that in tetrahydropyran rings. For instance, 4‴-OH radical contained the positive charges at carbons C-1‴, C-3‴, and C-5‴, and the negative ones at carbon C-2‴ and C-6‴. By means of this, aromatic rings will facilitate radical reactions better than saturated rings. In another approach, the spin density at the O atom shows the same trend as the BDE values [20, 21]. Herein, 3-O• and 3″-O• have contained the highest charges of 0.898 and 0.911, respectively. Therefore, it is desirable that the BDE values of the aromatic-linked OH groups will be lower.

The Fukui numbers are also a helpful tool to view electronics and reaction sites of each atom. Electrophilic sites have been generally deduced from $\Delta f_x = f_x^+ - f_x^- > 0$, and nucleophilic property is in association with $\Delta f_x < 0$ [35]. Considering the OH groups (Table S3), $\Delta f_x > 0$ is found at 3-OH, 5-OH, 3′-OH, 4′-OH, and 5″-OH, while the remainders are accompanied with $\Delta f_x < 0$. Importantly, the atom with the negative $f_x^o$ is always appropriate for

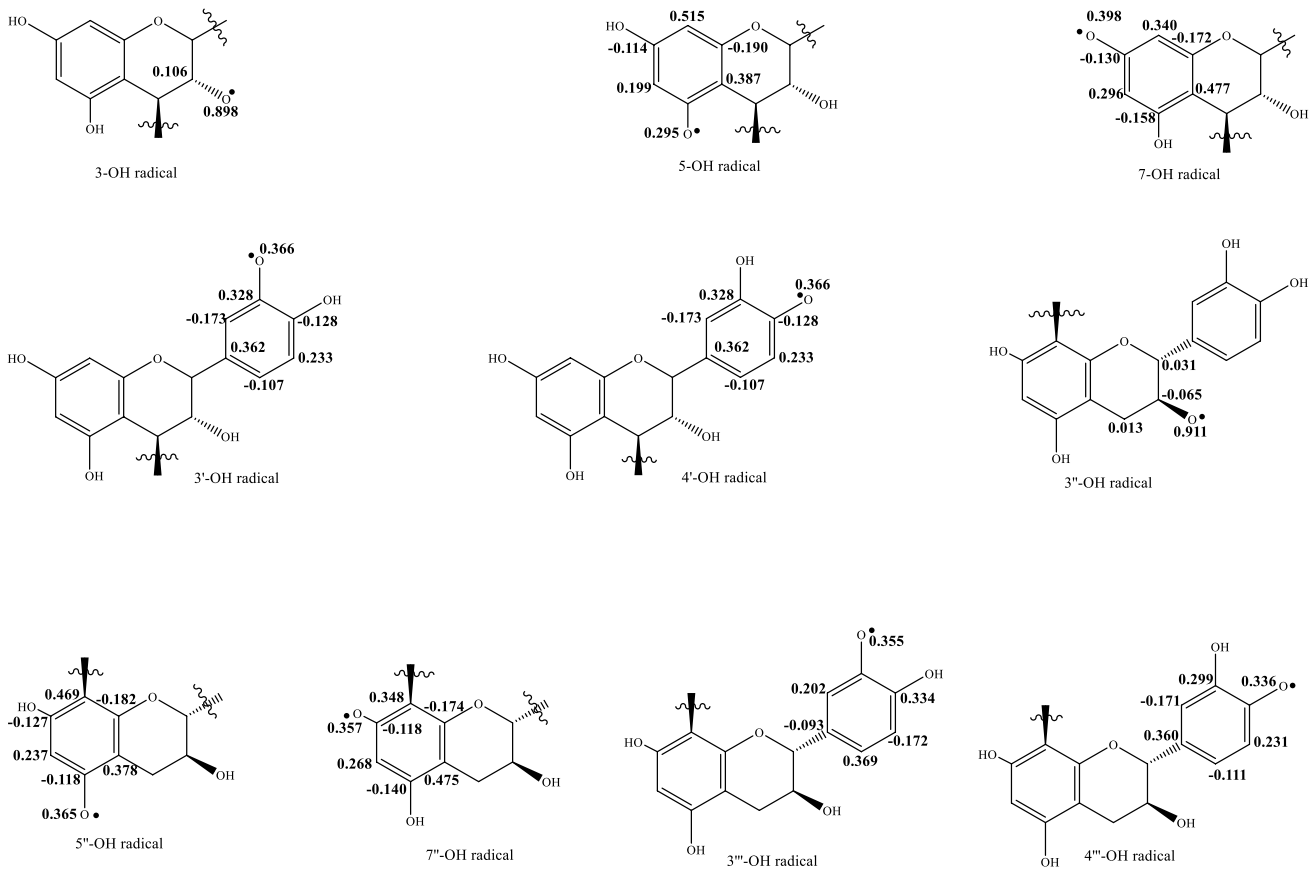


**Fig. 4** Spin density distribution of structural radicals in the gaseous medium at the theoretical M06-2X/6-311G(d,p) level

radical reactions [35]. Except for C3, C4, C5, C8a, C2″-O, C3″, C8″, C6‴, and H atoms, the remaining atoms, especially in terms of OH groups, are active sites to capture free radicals.

## Antioxidant mechanisms

### The HAT route

The reaction enthalpy BDE values are greatly dependent on environmental and structural factors. In the line with the above findings of spin density, at the M062x/6-311G(d.p) level, the highest BDE values of 103.9–106.8 kcal/mol are assigned to 3-OH and 3″-OH in both four studied mediums, whereas aromatic-linked OH groups possess the lower BDE values of 83.5–86.7 kcal/mol (Table 1). In each medium, the lowest BDE value belongs to 3′-OH (gas [80.9 kcal/mol], benzene [83.2 kcal/mol], methanol, and water [83.4 kcal/mol]). 4‴-OH is one of the group to exert the significant BDE values of 83.4 and 83.5 kcal/mol in water and methanol, respectively. The BDE values of 3-OH, 5-OH, and 7-OH are found to be mostly unchanged when converted gas into solvents. However, in contrast to 3′-OH, 3″-OH, and 5″-OH, the BDE values of 4′-OH, 3‴-OH, and 4‴-OH increase with the increase of polarity of mediums.

### The SET-PT and SPL-ET routes

The AIP value would help to consider the SET step, as well as it is the key element to decide the SET-PT route [19–23]. As can be seen from Table 1, the AIP values run following order: gas (168.0 kcal/mol) > benzene (150.4 kcal/mol) > methanol (120.0 kcal/mol) > water (115.0 kcal/mol). It is possible to deduce that ambient polarity has a significant impact on the charge species. The second step of the SET-PT route is represented by energy for proton dissociation, commonly known as the PDE. Alcoholic medium seems to promote deprotonation since the PDE energy of each OH group is arranged in the order as gas ≫ benzene > water > methanol. In the same BDE trend, the highest PDE values are owned by 3-OH and 3″-OH in each medium, whereas 3′-OH, once again, is found to have the lowest PDE values, especially in methanol (8.10 kcal/mol) and water (12.4 kcal/mol). 4‴-OH causes for the remarkable PDE values of 13.9 and 9.7 kcal/mol in water and methanol, respectively. It is further observed that the PDE values of OH groups of two phenyl rings are always lower than those of OH groups of chromene rings.

SPL-ET, the third mechanism, might be a viable route for the antioxidative effect of naturally occurring chemicals, particularly in solvents [19, 35]. The PA value is in charge

**Table 1** The reaction enthalpies at 298 K of PB1 at the theoretical M06-2X/6-311G(d,p) level (kcal/mol)

| No | BDE | | | | AIP | | | | PDE | | | |
|---|---|---|---|---|---|---|---|---|---|---|---|---|
| | Gas | Water | $CH_3OH$ | Benzene | Gas | Water | $CH_3OH$ | Benzene | Gas | Water | $CH_3OH$ | Benzene |
| 3-OH | 106.8 | 106.5 | 106.6 | 106.8 | 168.0 | 115.0 | 120.0 | 150.4 | 252.2 | 35.5 | 31.3 | 54.4 |
| 5-OH | 86.0 | 86.7 | 86.7 | 86.3 | | | | | 231.3 | 15.7 | 11.3 | 33.9 |
| 7-OH | 88.2 | 88.5 | 88.5 | 88.1 | | | | | 233.6 | 17.5 | 13.2 | 35.7 |
| 3′-OH | 80.9 | 83.4 | 83.4 | 83.2 | | | | | 226.2 | 12.4 | 8.1 | 31.6 |
| 4′-OH | 87.8 | 85.3 | 85.4 | 86.7 | | | | | 232.1 | 14.3 | 10.1 | 34.3 |
| 3″-OH | 103.9 | 105.1 | 105.1 | 104.4 | | | | | 249.2 | 34.1 | 29.7 | 52.0 |
| 5″-OH | 86.5 | 88.1 | 88.0 | 87.0 | | | | | 231.8 | 17.1 | 12.7 | 34.6 |
| 7″-OH | 85.8 | 85.8 | 85.8 | 85.8 | | | | | 232.7 | 16.3 | 12.0 | 35.0 |
| 3‴-OH | 86.6 | 85.7 | 85.7 | 86.0 | | | | | 233.4 | 16.2 | 11.8 | 35.2 |
| 4‴-OH | 85.6 | 83.4 | 83.5 | 84.8 | | | | | 232.4 | 13.9 | 9.7 | 34.0 |
| No | PA | | | | ETE | | | | | | | |
| | Gas | Water | $CH_3OH$ | Benzene | Gas | Water | $CH_3OH$ | Benzene | | | | |
| 3-OH | 365.2 | 72.9 | 70.5 | 128.3 | 54.9 | 77.6 | 80.8 | 76.6 | | | | |
| 5-OH | 311.5 | 41.5 | 37.9 | 82.2 | 92.7 | 86.8 | 88.9 | 112.7 | | | | |
| 7-OH | 330.1 | 49.4 | 46.3 | 96.5 | 71.5 | 83.1 | 86.9 | 89.6 | | | | |
| 3′-OH | 340.5 | 53.5 | 50.7 | 105.2 | 53.7 | 73.9 | 77.5 | 76.7 | | | | |
| 4′-OH | 350.9 | 57.5 | 54.9 | 112.9 | 50.2 | 71.8 | 75.2 | 71.8 | | | | |
| 3″-OH | 360.0 | 71.0 | 68.3 | 123.5 | 57.2 | 78.0 | 81.5 | 78.9 | | | | |
| 5″-OH | 326.4 | 48.8 | 45.6 | 94.4 | 73.4 | 83.3 | 87.1 | 90.6 | | | | |
| 7″-OH | 327.4 | 48.4 | 45.4 | 95.3 | 73.3 | 82.9 | 86.7 | 90.0 | | | | |
| 3‴-OH | 312.5 | 38.0 | 34.8 | 82.1 | 88.9 | 93.1 | 97.1 | 103.5 | | | | |
| 4‴-OH | 328.4 | 41.8 | 39.1 | 93.3 | 72.0 | 87.1 | 88.7 | 91.0 | | | | |

of the route's first step. As shown in Table 1, the PA values have the same tendency as the PDE values, by which the PA value of each OH group has been drastically increased in gas, but gets the lowest value in methanol. It evidently confirmed that medium polar solvents greatly support deprotonation. In each medium, similar to the BDE and PDE trends, the highest PA values are assignable to 3-OH and 3″-OH. However, the lowest PA values of 34.8 and 38.0 kcal/mol are caused by 3‴-OH in methanol and water, respectively. Our result shows an agreement with the analogous publications. As a representative example, Chang et al. (2019) suggested that in the increasing polar solvents, like ethanol, water, formic acid, acetic acid, and lactic acids, the PA values of OH groups of *N*-glycolylneuraminic and *N*-acetylneuraminic acids were often found lower than those in gas and benzene [36].

The second step of the SPL-ET route involved in the electron transfer process, which is possibly understandable by the ETE enthalpy analysis. The lowest ETE value of 50.2 kcal/mol belongs to 4′-OH in gas, while the highest ETE values of 112.7 and 103.5 kcal/mol are due to the action of 5-OH and 3‴-OH in benzene, respectively. It is also found that in each studied medium, 4′-OH possesses the lowest ETE values, whereas 5-OH and 3‴-OH always generate the highest values. Similar to the analogous report, the ETE values have generally increased solvents, especially in weak polar solvents, such as benzene, but they decrease in nonpolar medium [36, 37]. Hence, it is safely argued that environmental gas supports electron transfer processes.

### Favorable mechanisms

The favorable antioxidant route of the studied compound PB1 has been possibly unraveled by a comparison of enthalpy results. The HAT, SET-PT, and SPL-ET routes will be decided by the BDE, AIP, and PA values, respectively [19–23]. By this approach, the minimum among these three enthalpies is expected. From Table 1, the PA values in the studied solvents, especially in medium polar solvent methanol, are substantially lower than the AIP and BDE values (PA ≪ AIP < BDE). When comparing them, it appears that in solvent the SPL-ET route is a preferentially antioxidative route for compound PB1. In turn, considering the gaseous environment, the BDE values are found lower than the AIP and PA values (BDE < AIP ≪ PA). It suggested that the HAT is favorable.

### Kinetic study

The HOO• radical, often known as hydrogen superoxide, is a protonation form of superoxide. This species existed in both atmosphere and living cells. It mainly causes reactive oxygen species [38]. In this section, we consider the kinetic interactions between the most active sites of molecule PB1 and HOO• radicals. To date, no publication has addressed this aspect before.

At the M062X/6-311G(d,p) theoretical level, the calculations were carried out in two mediums gas and methanol. The results were outlined in Table 2 and Figs. 5 and S3. Previous publications revealed that the free radical reaction will be stable and faster with the higher $K$ and the lower $\Delta G^{\#}$ [19–23, 35]. Taking the gaseous results into consideration, similar to the BDE outcomes, 3′-OH + HOO• has established the lowest $\Delta G^{\#}$ value of 11.1 kcal/mol, and the highest $K$ value of $6.738 \times 10^7$ L/mol s (Table 2). 5-OH + HOO• is characteristic with the significant $\Delta G^{\#}$ value of 16.8 kcal/mol, and the $K$ value of $1.689 \times 10^5$ L/mol s. 4′-OH, 3‴-OH, and 4‴-OH interacted with HOO• resulting in the $\Delta G^{\#}$ values of 17.3–19.3 kcal/mol, and the $K$ values of $1.158–6.278 \times 10^4$ L/mol s. The RE (relative energy) at TS (transition state) showed the same trend with the $\Delta G^{\#}$ and $K$ values, in which an arrangement run as 3′-OH < 5-OH < 4‴-OH < 4′-OH < 3‴-OH (Fig. 5).

The $\Delta G^{\#}$ values are higher, but the $K$ values are lower, as converted gas into methanol (Table 5). The highest $\Delta G^{\#}$ increase of 6.20 kcal/mol is found in 3′-OH + HOO•. Significantly, the methanolic $K$ value of 3′-OH + HOO• is less than that in gas by about 1000 times. Likewise, 5-OH + HOO• induces the $K$ value lower than that in gas by 100 times. In methanol, OH groups at carbons C-3′, C-4′, and C-4‴ are the most active centers with the $\Delta G^{\#}$ values of 17.7–18.8 kcal/mol, and the $K$ values of $1.981–9.404 \times 10^4$ L/mol s. Coinciding with the $\Delta G^{\#}$ and $K$ values, the methanolic RE values are followed in a clear order of 4‴-OH < 3′-OH < 4′-OH < 5-OH < 3‴-OH.

### Metal complex chelation

Another antioxidant mechanism of flavonoids could be the formation of complexes between metal ions and polyphenol-type flavonoids that prohibit these metal ions from participating in the free radical production [39]. Furthermore, natural metal

**Table 2** The calculated $\Delta G^{\#}$ and $K$ for HOO• radical attack in gas and methanol at the theoretical M06-2X/6-311G(d,p) level

| Position | $\Delta G^{\#}$ (kcal/mol) Gas | $K$ (L/mol s) | $\Delta G^{\#}$ (kcal/mol) Methanol | $K$ (L/mol s) |
|---|---|---|---|---|
| 5-OH | 16.8 | $1.689 \times 10^5$ | 20.2 | $4.769 \times 10^3$ |
| 3′-OH | 11.1 | $6.738 \times 10^7$ | 17.8 | $8.829 \times 10^4$ |
| 4′-OH | 18.9 | $1.765 \times 10^4$ | 18.8 | $1.981 \times 10^4$ |
| 3‴-OH | 19.3 | $1.158 \times 10^4$ | 20.4 | $3.706 \times 10^3$ |
| 4‴-OH | 17.3 | $6.278 \times 10^4$ | 17.7 | $9.404 \times 10^4$ |

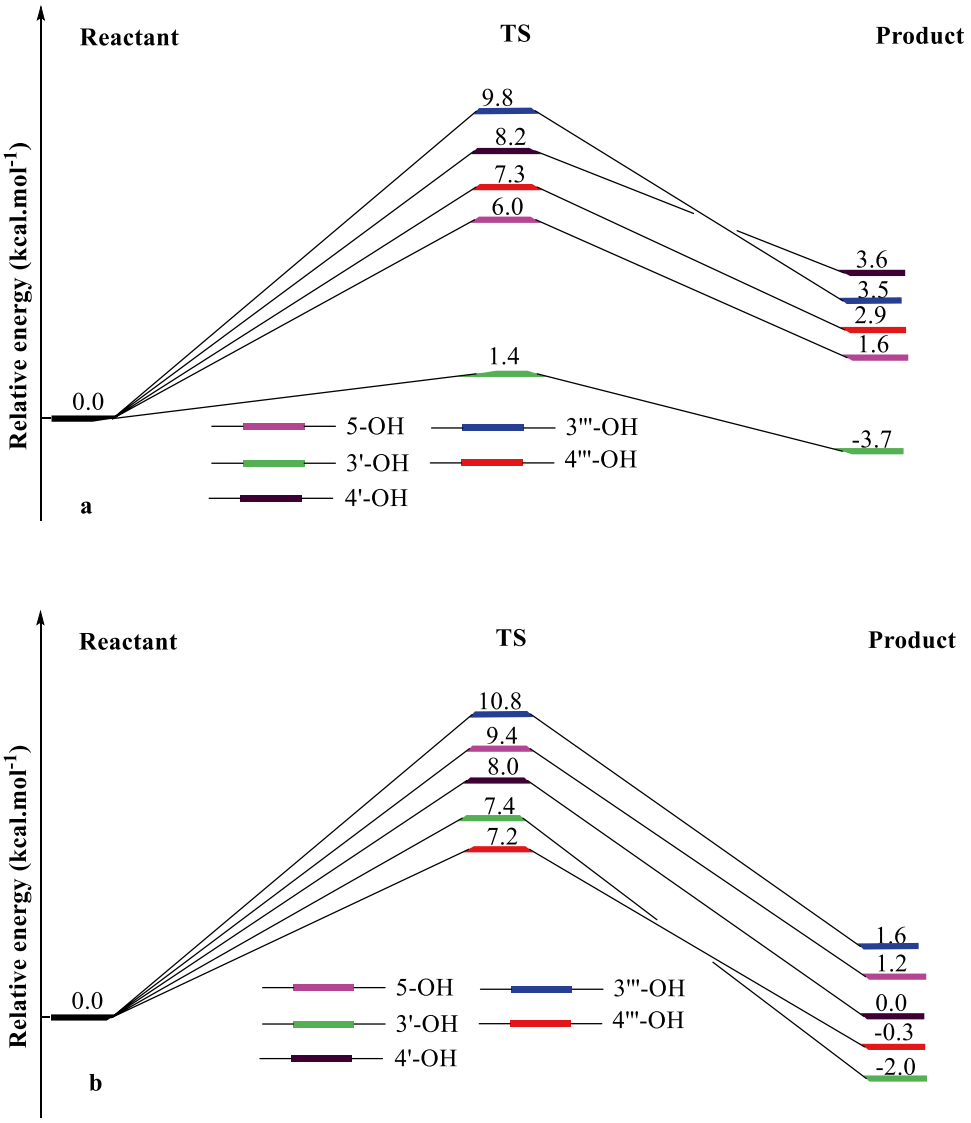


**Fig. 5** Energy diagram for the reaction of HOO• radical attack in gas (**a**) and methanol (**b**) at the theoretical M06-2X/6-311G(d,p) level

chelators, such as flavonoids, should be preferred over synthetic chelators, which have toxicity [39]. From the PA result and the favorable space position between 3‴-OH and 4‴-OH, we continue to propose and compare two chelated models $Cu(PB1)_2$ and $Zn(PB1)_2$ since $Cu^{2+}$ and $Zn^{2+}$ were frequently used in both experimental and theoretical chelated studies [19, 37, 39, 40]. The comparison is mostly based on three criteria, including the binding energy (BE), and FMO and UV–Vis analyses. In methanol, the BE and FMO values have been calculated at the M062X/6-31G(d,p)/LANL2DZ theoretical level, while the UV–Vis spectral data were obtained using the TD-DFT/M062X/6-31G(d,p)/LANL2DZ theoretical level (Table 3 and Fig. 6). The BE parameter reflects the stability of a complex, which is calculated following the equation below [41].

**Table 3** Binding energy (kcal/mol) and FMO analysis for complexes $Cu(PB1)_2$ and $Zn(PB1)_2$ in methanol at the theoretical M06-2X/6-31G(d,p)/LANL2DZ level and UV–Vis analysis in methanol at the theoretical TD-DFT/M06-2X/6-31G(d,p)/LANL2DZ level

| No | Binding energy | FMO | | | UV–Vis | | | |
|---|---|---|---|---|---|---|---|---|
| | BE | $\varepsilon_{HOMO}$ (eV) | $\varepsilon_{LUMO}$ (eV) | $\varepsilon_{gap}$ (eV) | $\lambda_{max}$ (nm) | $E_{vert}$ (eV) | Oscillator strength *f* | Excitation transition |
| $Cu(PB1)_2$ | −112.104 | −7.431 | −2.759 | 4.672 | 488 | 2.536 | 0.032 | H-2→L (74%) |
| $Zn(PB1)_2$ | −59.187 | −6.536 | −00.034 | 7.337 | 203 | 6.115 | 0.523 | H-4→L (12%) |

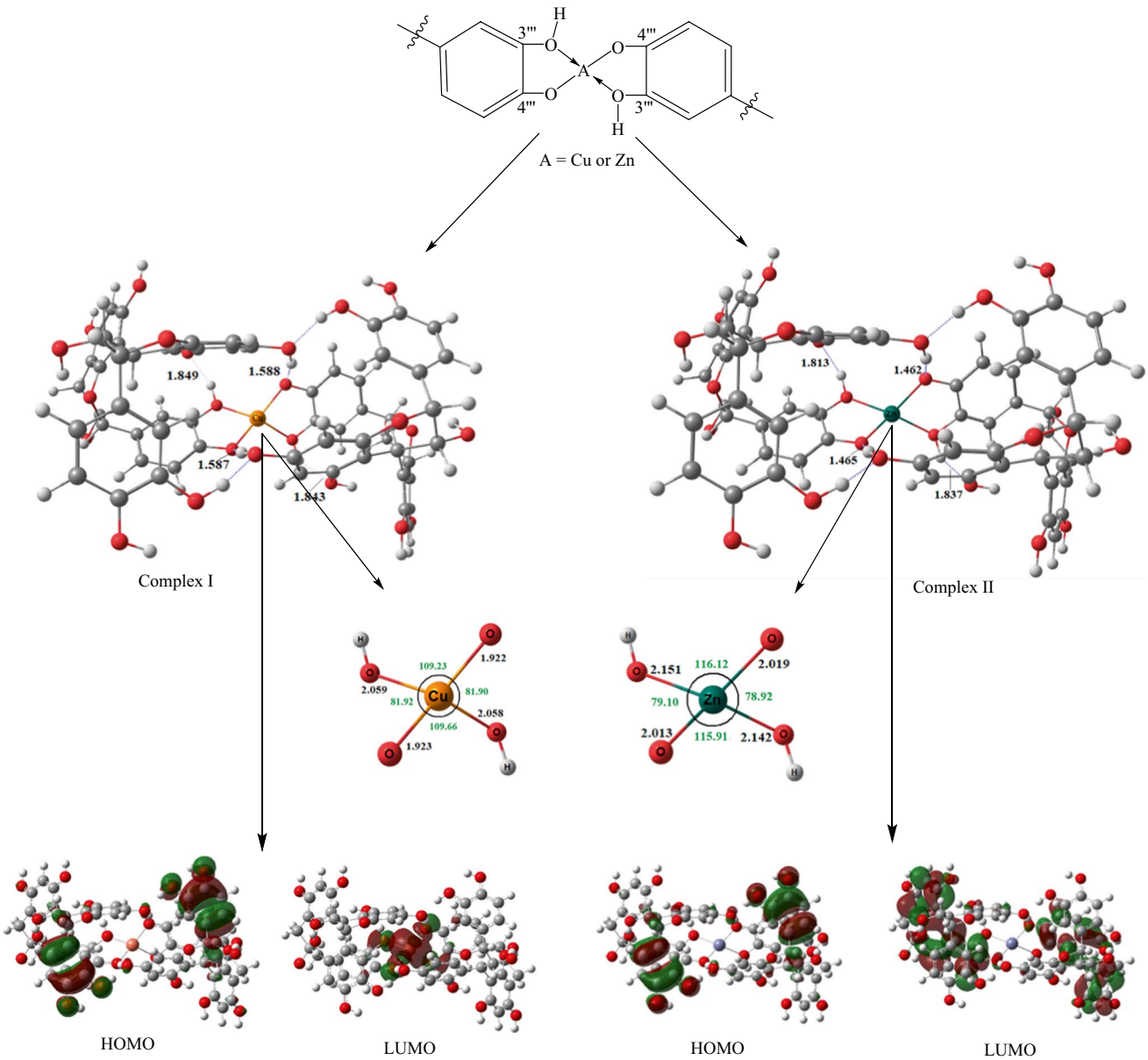


**Fig. 6** The optimized complex I: $Cu(PB1)_2$ and complex II: $Zn(PB1)_2$ and their FMO in methanol at the theoretical M06-2X/6-31G(d,p)/LANL2DZ level

$$BE = -[E_{complex} - (E_{metal} + 2E_{ligand})]/2 \quad (14)$$

where $E_{complex}$, $E_{metal}$, and $E_{ligand}$ stand for the energy of complex, metal ion, and flavonoid ligand, respectively. As shown in Table 3, $Cu(PB1)_2$ complex with the BE value of − 112.104 kcal/mol is more stable than $Zn(PB1)_2$ complex (BE = − 59.187 kcal/mol). Almost Cu–O bond lengths are shorter than those of Zn–O (Fig. 6). HOMO illustrations of two complexes are not different. However, the electrons are found to highly concentrate around Cu atom in LUMO of $Cu(PB1)_2$ complex, but they completely delocalize in two PB1 molecules in LUMO of $Zn(PB1)_2$ complex. Band gap energy $\varepsilon_{gap}$ of $Cu(PB1)_2$ complex is lower than that of $Zn(PB1)_2$ complex by 2.665 eV. At the TD-DFT/M062X/6-31G(d,p)/LANL2DZ theoretical level, the $Cu(PB1)_2$ complex formation has given rise a long-wavelength peak at $\lambda_{max}$ 488 nm (vertical transition energy $E_{vert} = 2.536$ eV, oscillator strength $f = 0.032$, and excitation transition H-2 → $L$ [74%]). In contrast, the formation of $Zn(PB1)_2$ complex results in a short-wavelength peak at $\lambda_{max}$ 488 nm ($E_{vert} = 6.115$ eV, $f = 0.523$, and H-4 → $L$ [12%]).

## Molecular docking studies

Tyrosine enzyme is the rate-limiting enzyme involved in the synthesis of melanin [42]. In the recent years, the tyrosinase inhibition in melanin synthetic pathway has attracted interests to the search for skin-whitening agents. In this scenario, the molecular docking simulation was conducted to clarify the antioxidative mechanism PB1 against human tyrosinase enzyme (PDB ID: 5M8M). The co-crystallized ligand, kojic acid (KA), was re-docked to the binding site of the targeted enzyme to validate the accuracy of the docking procedure. Molecular docking is a useful tool to quickly find, for each protein interacting with the ligand, the optimal value of the score function. The objective of any docking calculation is to find the best pose, which corresponds to the lowest energy [43–45]. The docking result is considered reliable when the RMSD value does not exceed 2.0 Å. In this study, the docked pose of KA with the lowest binding free energy was compared with its native structure based on its RMSD value, which was 0.215 Å (Fig. 7). This result suggests that the procedure and the set parameters were reproducible and appropriate for further docking simulation.

The inhibitory potential of PB1 against human tyrosinase enzyme was then investigated. According to the ranking criteria of Autodock4, the more the negative value of the docking scores, the higher the binding affinity of the compound towards receptor is targeted [46, 47]. The obtained results indicated that reference ligand KA docked to human tyrosinase enzyme with a dock score of − 10.57 kcal/mol. Thus, PB1 with a dock score of − 12.84 kcal/mol would be considered as a potential inhibitor. The binding free energies, interaction type, and residues participating in interaction are tabulated in Table 4. Binding orientation analysis of KA indicated a $\pi$-$\pi$ stacked interaction with His381; meanwhile, His192, His377, and Thr391 were the main residues involved in van der Waal binding types. The interaction was further stabilized with one H bond with Ser394. Regarding compound PB1, an array of hydrogen bonds was observed as contributed by Val196, Glu216, Tyr362, Arg374, Gly389, and Ser394. It also initiated van der Waals and $\pi$-$\pi$ stacked interaction with Thr391 and His381, respectively (Fig. 8). Remarkably, OH groups of two phenyl rings directly participated forming hydrogen bonds with the essential residues which contributed to the malfunction of the targeted enzyme. These results imply that PB1 might effectively inhibit the human tyrosinase enzyme.

**Table 4** Binding free energy and residues interactions of PB1 and KA (kojic acid) against human tyrosinase enzyme

| Ligand | Binding free energy (kcal/mol) | Binding interaction | Residues |
|---|---|---|---|
| PB1 | − 12.84 | H bond | Val196, Glu216, Tyr362, Arg374, Gly389, Ser394 |
| | | van der Waals | Thr391 |
| | | $P_i$ interaction | His381 ($\pi$-$\pi$ stacked) |
| KA | − 10.57 | H bond | Ser394 |
| | | van der Waals | His192, His377, Thr391 |
| | | $P_i$ interaction | His381 ($\pi$-$\pi$ stacked) |

The attrition rates of therapeutic compounds during clinical development are becoming lesser nowadays (around 8%) due to prior attention to ADMET properties [48]. Molecules with useful physicochemical properties and a low level of toxicity are highly desirable. In this study, Molinspiration and ProTox-II were utilized to evaluate the drug-like properties and the acute toxicity of the studied compounds (Table 5). A molecule with a higher number of rotatable bonds becomes more flexible, and has a good binding

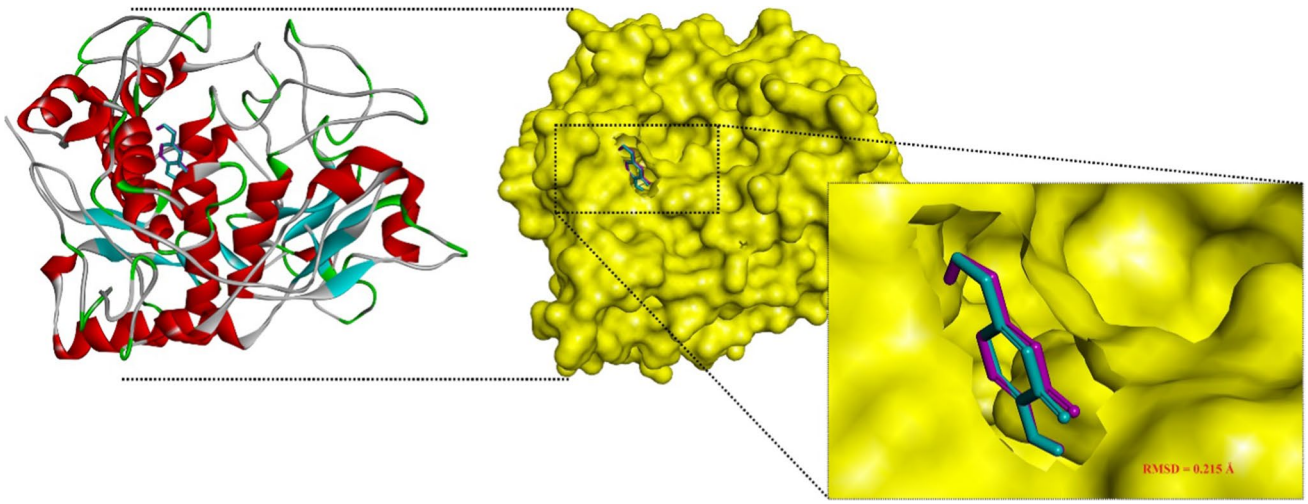


**Fig. 7** Dock pose of studied KA (blue) and native KA (magenta) in the active site of human tyrosinase enzyme (PDB ID: 5M8M)

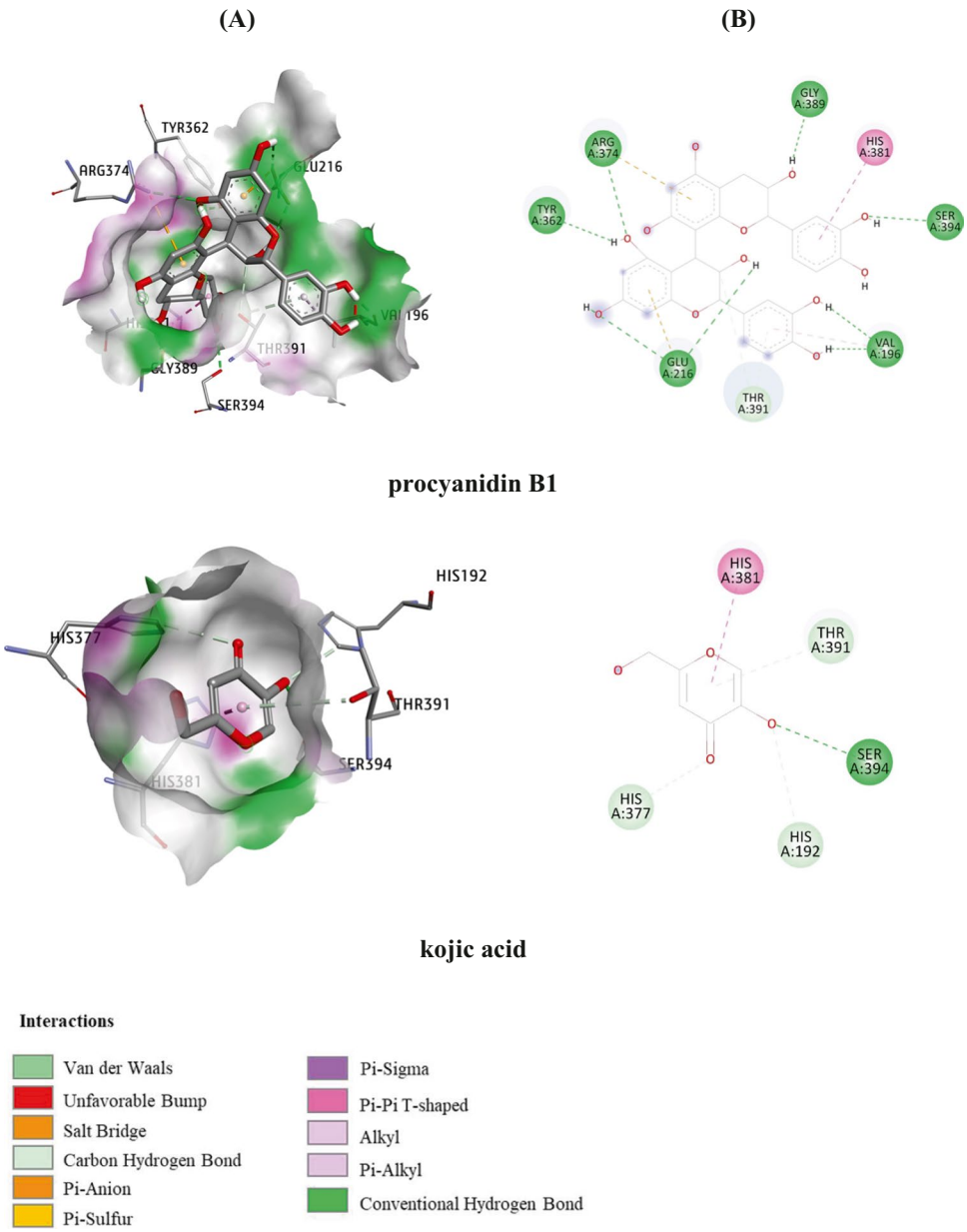


**Fig. 8** Docking conformation of PB1 and KA in the human tyrosinase enzyme suggested by molecular docking studies

**Table 5** Molecular properties of PB1 and KA

| Property | PB1 | KA |
|---|---|---|
| TPSA (Å$^2$) | 220.76 | 70.67 |
| MW | 578.52 | 142.11 |
| NRB | 3 | 1 |
| Predicted $LD_{50}$ (mg/kg) | 2500 | 550 |
| Predicted toxicity class* | 5 | 3 |

TPSA: topological polar surface area; MW: molecular weight; NRB: number of rotatable bond

*Toxicity prediction class: 1 → 6 (high toxicity to nontoxic)

affinity with the binding pocket [49]. The obtained data of PB1 and KA are in line with this statement, of which PB1 has three rotatable bonds (NRB), and KA has only one NRB. In addition, PB1 was classified in a low-toxic class (class 5), as compared to KA (class 3), thereby suggesting its potential in the later drug development stages.

## Conclusion

For the first time, our current paper applies the DFT calculated approach to investigate the antioxidant effect of molecule PB1. The antioxidant potential is caused by the actions of OH groups, which might be explained by geometrical and electronic analyses.

The calculation at the M062X/6-311G(d,p) theoretical level indicated that the HAT route is favorable for this flavonoid in the gaseous phase, and the lowest BDE value of 80.9 kcal/mol is assigned to 3′-OH. However, in polarity solvents, the SPL-ET route is appropriate for this compound, and the lowest PA value of 34.8 kcal/mol is of 3‴-OH in methanol. In gas, 3′-OH + HOO• generates the lowest $\Delta G^{\#}$ value of 11.1 kcal/mol, and the highest $K$ value of $6.738 \times 10^7$ L/mol s. Meanwhile, 3′-OH + HOO• and 4‴-OH + HOO• establish the significant $\Delta G^{\#}$ and $K$ values in methanol. Metal chelation is another approach to elucidate the antioxidant activity of compound PB1, in which complex formation of this molecule with $Cu^{2+}$ induces the BE value about 2.0 times lower than that of this molecule with $Zn^{2+}$. Molecular docking simulation further highlighted the antioxidant activity of PB1 through potential human tyrosinase enzyme inhibitory mechanism with the high binding affinity (−12.84 kcal/mol) and interaction with key residues within the active site.

**Supplementary Information** The online version contains supplementary material available at https://doi.org/10.1007/s00894-022-05354-x.

**Author contribution** P. T. Thuy and P. M. Quan: formal analysis, D. X. Duc: revised manuscript, and N. T. Son: designated and wrote manuscript. All authors reviewed the manuscript.

**Data availability** The data that support the findings of this study are available from the corresponding author upon reasonable request.

## Declarations

**Conflict of interest** The authors declare no competing interests.

## References


1. Murray MT (2020) Procyanidolic oligomers, Textbook of natural medicine (2nd ed) Churchill Livingstone, 823–828
2. Enomoto T, Nagasako-Akazome Y, Kanda T et al (2006) Clinical effects of apple polyphenols on persistent allergic rhinitis: a randomized double-blind platebo-controlled parallel arm study. J Investig Allergol Clin Immunol 16:283–289
3. Yang J, Xiao YY (2013) Grape phytochemicals and associated health benefits. Crit Rev Food Sci Nutr 53:1202–1225. https://doi.org/10.1080/10408398.2012.692408
4. Duda-Chodak A, Tarko T, Sroka P et al (2010) The profile of polyphenols and antioxidant properties of selected appled cultivars grown in Poland. J Fruit Ornam Plant Res 18:39–50
5. Saint-Cricq N, Provost C, Vivas N (1999) Comparative study of polyphenol scavenging activities assessed by different methods. J Agric Food Chem 47:425–431. https://doi.org/10.1021/jf980700b
6. Rodrigo I, Loreto C, Pia R et al (2011) Postharvest sensory and phenolic characterization of 'elegant laday' and carson' peaches. Chil J Agric Res 71:445–451
7. Gupta RC, Srivastava A, Sinha A et al (2019) Biomarkers of foods and nutraceuticals: applications in efficacy, safety, and toxicity. In: Gupta R., Srivastava A., Lall R. (eds) Nutraceuticals in Veterinary Medicine. Springer, Germany
8. Villano D, Fernandez-Pachon MS, Moya ML et al (2007) Radical scavenging ability of polyphenolic compounds towards DPPH free radical. Talanta 71:230–235. https://doi.org/10.1016/j.talanta.2006.03.050
9. Soobrattee MA, Neergheen VS, Luximon-Ramma A et al (2005) Phenolics as potential antioxidant therapeutic agents: mechanism and actions. Mutat Res 579:200–213. https://doi.org/10.1016/j.mrfmmm.2005.03.023
10. Karrouchi K, Fettach S, Jotani MM et al (2020) Synthesis, crystal structure, Hirshfeld surface analysis, DFT calculations, anti-diabetic activity and molecular docking studies of (E)-N′-(5-bromo-2-hydroxybenzylidene) isonicotinohydrazide. J Mol Struct 1221:128800. https://doi.org/10.1016/j.molstruc.2020.128800
11. Gatfaoui S, Sagaama A, Issaoui N et al (2020) Synthesis, experimental, theoretical study and molecular docking of 1-ethylpiperazine-1,4-diium bis(nitrate). Solid State Sci 106:106326. https://doi.org/10.1016/j.solidstatesciences.2020.106326
12. Noureddiine O, Issaoui N, Medimagh M et al (2021) Quantum chemical studies on molecular structure, AIM, ELF, RDG and antiviral activities of hybrid hydroxychloroquine in the treatment of COVID-19: molecular docking and DFT calculations. J King Saud Univ Sci 33:1011334. https://doi.org/10.1016/j.jksus.2020.101334
13. Kazachenko AS, Akman F, Abdelmoulahi H et al (2021) Intermolecular hydrogen bonds interactions in water clusters of ammonium sulfamate: FTIR, X-ray diffraction, AIM, DFT, RDG, ELF. NBO analysis J Mol Liq 342:117475. https://doi.org/10.1016/j.molliq.2021.117475
14. Sagaama A, Brandan SA, Issa TB et al (2020) Searching potential antiviral candidates for the treatment of the 2019 novel coronavirus based on DFT calculations and molecular docking. Heliyon 6:e04640. https://doi.org/10.1016/j.heliyon.2020.e04640
15. Huang HC, Chang TY, Chang LZ et al (2012) Inhibition of melanogenesis versus antioxidant properties of essential oil extracted from leaves of *Vitex negundo* Linn and chemical composition analysis by GC-MS. Molecules 17:3902–3916. https://doi.org/10.3390/molecules17043902
16. Pintus F, Matos MJ, Vilar S et al (2017) New insights into highly potent tyrosinase inhibitors based on 3-heteroarylcoumarins: anti-melanogenesis and antioxidant activities, and computational molecular modeling studies. Bioorg Med Chem 25:1687–1695. https://doi.org/10.1016/j.bmc.2017.01.037
17. Maciej S, Andrzej G, Zbigniew S (2021) A statistically supported antioxidant activity DFT benchmark—the effects of Hartree-Fock exchange and basis set selection on accuracy and resources uptake. Molecules 26:5058. https://doi.org/10.3390/molecules26165058
18. Frisch MJ, Trucks GW, Schlegel HB et al (2010) GAUSSIAN 09 (revision C.01) Inc., Wallingford CT
19. Thuy PT, Son NT (2021) Thermodynamic studies on antioxidative action of cynandione A: a DFT approach. Struct Chem 32:1807–1817. https://doi.org/10.1007/s11224-021-01756-4
20. Trang NV, Thuy PT, Thanh DTM et al (2021) Benzofuran-stilbene hybrid compounds: an antioxidant assessment — a DFT study. RCS Adv 11:12971–12980. https://doi.org/10.1039/D1RA01076J
21. Thuy PT, Trang NV, Son NT (2020) Antioxidant of 2-phenylbenzofuran derivatives: structural-electronic effects and mechanisms. RCS Adv 10:6315–6332. https://doi.org/10.1039/C9RA10835A
22. Son NT, Thanh DTM, Trang NV (2019) Flavone norartocarpetin and isoflavone 2′-hydroxygenistein: a spectroscopic study for structure, electronic property and antioxidant potential using DFT (density functional theory). J Mol Struct 1193:76–88. https://doi.org/10.1016/j.molstruc.2019.05.016
23. Thuy PT, Trang NV, Duc DX, Son NT (2021) The antioxidative potential of benzofuran-stilbene hybrid derivatives: a comparison between natural and synthetic compounds. Struct Chem 32:2271–2281. https://doi.org/10.1007/s11224-021-01802-1

24. Anh LTT, Son NT, Van Tuyen N et al (2022) Antioxidative and α-glucosidase inhibitory constituents of *Polyscias guilfoylei*: experimental and computational assessments. Mol Divers 26:229–243. https://doi.org/10.1007/s11030-021-10206-6
25. Lagorce D, Pencheva T, Villoutreix BO et al (2009) DG-AMMOS: a new tool to generate 3D conformation of small molecules using distance geometry and automated molecular mechanics optimization for in silico screening. BMC Chem Biol 9:6. https://doi.org/10.1186/1472-6769-9-6
26. Allouche AR (2011) Gabedit—a graphical user interface for computational chemistry softwares. J Comput Chem 32:174–182. https://doi.org/10.1002/jcc.21600
27. Lai X, Wichers HJ, Soler-Lopez M et al (2017) Structure of human tyrosinase related protein 1 reveals a binuclear zinc active site important for melanogenesis. Angew Chem Int Ed Engl 56:9812–9815. https://doi.org/10.1002/anie.201704616
28. Choi I, Park Y, Ryu IY et al (2021) In silico and in vitro insights into tyrosinase inhibitors with a 2-thioxooxazoline-4-one template. Computat Struct Biotechnol J 19:37–50. https://doi.org/10.1016/j.csbj.2020.12.001
29. Sharmila CM, Devi RC, Sureka A et al (2019) In silico analysis of the effect of vasicine and vasinone against human tyrosinase receptor in the management of hyperpigmentation of skin diseases. Asian J Pharm Pharmacol 5:518–524. https://doi.org/10.31024/ajpp.2019.5.3.13
30. Roselan MA, Zakaria N, Nur HF et al (2021) A preliminary study: molecular docking, optimization and characterization of kojic monooleate nanoemulsion for cosmeceuticals application. J Sustain Sci Manag 16:158–176. https://doi.org/10.46754/jssm.2021.12.011
31. Firmansyah D, Sumiwi SA, Saptarini NM et al (2021) Molecular interaction of curcumin, demethoxycurcumin, bisdemethoxycurcumin, tyrosinase and tyrosinase-related protein-1. Rasayan J Chem 14:2298–2303. https://doi.org/10.31788/rjc.2021.1446418
32. Boulebd H (2020) Theoretical insights into the antioxidant activity of moracin T. Free Radic Res 54:221–230. https://doi.org/10.1080/10715762.2020.1747616
33. Dung NT, Thanh DM, Huong NT et al (2020) Quinolone and isoquinolone alkaloids: the structural-electronic effects and the antioxidant mechanisms. Struct Chem 31:2435–2450. https://doi.org/10.1007/s11224-020-01602-z
34. Mohajeri A, Asemani SS (2009) Theoretical investigation on antioxidant activity of vitamins and phenolic acids for designing a novel antioxidant. J Mol Struct 930:15–20. https://doi.org/10.1016/j.molstruc.2009.04.031
35. Son NT, Thuy PT, Trang NV (2021) Antioxidative capacities of stilbenoid Suaveolensone A and flavonoid Suaveolensone B: A detailed analysis of structural-electronic properties and mechanisms. J Mol Struct 1224:129025. https://doi.org/10.1016/j.molstruc.2020.129025
36. Rui C, Bowen Y, Qiu-Jin Z (2019) Theoretical studies on the electronic structure parameters and reactive activity of Neu5Gc and Neu5Ac under food processing solvent environment. Molecules 24:313. https://doi.org/10.3390/molecules24020313
37. Thuy PT, Van Trang N, Duc DX et al (2021) The antioxidative potential of benzofuran-stilbene hybrid derivatives: a comparison between natural and synthetic compounds. Struct Chem 32:2271–2281. https://doi.org/10.1007/s11224-021-01802-1
38. Heard DE, Pilling MJ (2003) Measurement of OH and $HO_2$ in the troposphere. Chem Rev 103:5163–5198. https://doi.org/10.1021/cr020522s
39. Tereza FM, Lurdes MM, Helena FM et al (2002) Iron and copper chelation by flavonoids: an electrospray mass spectrometry study. J Inorg Biochem 92:105–111. https://doi.org/10.1016/S0162-0134(98)10037-5
40. Sabri AC, Nassima MS, Farid B et al (2016) In vitro antioxidant versus metal ion chelating properties of flavonoids: a structure-activity investigation. PLoS One 11:e0165575. https://doi.org/10.1371/journal.pone.0165575
41. Mohammad AM, Aftab AS et al (2021) The effects of oxidation states and spin states of chromium interaction with *Sargassum* sp.: a spectroscopic and density functional theoretical study. Green Sustain Chem 11:125–141. https://doi.org/10.4236/gsc.2021.114011
42. Bonaventure J, Domingues MJ, Larue L (2013) Cellular and molecular mechanisms controlling the migration of melanocytes and melanoma cells. Pigment Cell Melanoma Res 26:316–325. https://doi.org/10.1111/pcmr.12080
43. Ben Issa T, Sagaama A, Issaoui N (2020) Computational study of 3-thiophene acetic acid: molecular docking, electronic and intermolecular interactions investigations. Comput Biol Chem 86:107268. https://doi.org/10.1016/j.compbiolchem.2020.107268
44. Sagaama A, Noureddine O, Brandán SA et al (2020) Molecular docking studies, structural and spectroscopic properties of monomeric and dimeric species of benzofuran-carboxylic acids derivatives: DFT calculations and biological activities. Comput Biol Chem 87:107311. https://doi.org/10.1016/j.compbiolchem.2020.107311
45. Sagaama A, Issaoui N, Al-Dossary O et al (2021) Non covalent interactions and molecular docking studies on morphine compound. J King Saud Univ Sci 33:101606. https://doi.org/10.1016/j.jksus.2021.101606
46. Quan PM, Huong LTT, Toan TQ et al (2021) *Cannabis sativa* L. chemical compositions as potential plasmodium falciparum dihydrofolate reductase-thymidinesynthase enzyme inhibitors: an in silico study for drug development. Open Chem 19:1235–1241. https://doi.org/10.1515/chem-2021-0102
47. Ngo ST, Vu KB, Pham MQ et al (2021) Marine derivatives prevent wMUS81 in silico studies. R Soc Open Sci 8:9. https://doi.org/10.1098/rsos.210974
48. Bordoloi M, Saikia S, Kolita B et al (2018) Volatile inhibitors of phosphatidylinositol-3-kinase (PI3K) pathway: anticancer potential of aroma compounds of plant essential oils. Anticancer Agents Med Chem 18:87–109. https://doi.org/10.2174/1871520617666170327105706De
49. Oliveira AS, Llanes LC, Nunes RJ et al (2021) Antioxidant activity, molecular docking, quantum studies and in vivo antinociceptive activity of sulfonamides derived from carvacrol. Front Pharmacol 12:788850. https://doi.org/10.3389/fphar.2021.788850